Impact-induced vibration in vehicular driveline systems: theoretical and experimental investigations

Impact-induced vibration in vehicular driveline systems: theoretical and experimental investigations

M Gnanakumarr[1], **S Theodossiades**[1], **H Rahnejat**[1]*, and **M Menday**[2]
[1]Wolfson School of Mechanical and Manufacturing Engineering, University of Loughborough, Loughborough, UK
[2]Ford Engineering Research Centre, Dunton, Essex, UK

The manuscript was received on 30 July 2004 and was accepted for publication on 27 October 2004.

DOI: 10.1243/146441905X10023

Abstract: The paper investigates the conditions leading to the emergence and persistence of an acute metallic noise in light-truck drivelines. Sudden demands in torque in the presence of lash zones give rise to this phenomenon, which is onomatopoeically referred to as *clonk*. The study of clonk requires combined rigid multi-body dynamics and flexible body oscillations. The results show high-frequency contributions in the driveline vibrational response of certain structural modes of the driveshaft pieces, which are induced by remote impact of meshing transmission teeth through backlash. The numerically predicted spectrum of vibration shows good correlation with experimental measurements of radiated noise from a dynamic drivetrain rig.

Keywords: clonk phenomenon, high-frequency metallic noise, impact, backlash, elastodynamics, multi-body dynamics, power trains

1 INTRODUCTION

The noise, vibration, and harshness (NVH) spectrum of a typical vehicular driveline system contains contributions of a significant number of vibration components ranging from a few hertz to several kilohertz. Often these contributions have strong interaction effects, with shuffle and clonk being among the most interactive phenomena and two of the major concerns at extremes of the spectrum [**1**]. A short-duration audible high-frequency elasto-acoustic phenomenon, which occurs as a load reversal in the presence of lashes in the driveline, is known in the industry as *clonk* (300–5000 Hz) [**2**–**5**]. This load reversal is often induced by vibro-impact in the various lash zones in the drivetrain system (transmission, differential, or spline joints) through low-frequency torsional rigid body motion of the powertrain system, known as *shuffle* [**6**–**9**]. The rigid body motion of the driveline system is perceptible by vehicle passengers through a corresponding fore-and-aft longitudinal motion of the vehicle, known as *shunt* (2–8 Hz). Clonk may be heard on the first cycle of the shuffle response [**10**–**13**]. Shuffle and shunt may be induced by driver action or via road input. Driver action can include sudden throttle tip-in from coast to drive condition, or conversely through abrupt release of throttle, termed back-out, from drive to coast. Any sudden engagement of clutch in low gear and at low road speeds can also create shuffle and shunt, leading to clonk conditions. In all cases, the rise rate of the torque pulse has a steep gradient and is referred to as *jerk*. Its short duration acts as an impulse that excites a large number of structural modes of the lightly damped driveline system. The high-frequency content of the modal response propagates to the passengers' cabin through cabin floor (referred to as thud) or as air-borne noise, heard by occupants by echo from roadside obstacles when vehicle windows are lowered. In particular, the thin-walled components such as the driveshaft tubes and the transmission bell housing are effective noise radiators. Their vibration response and, hence, the externally radiated sound power are thought to be mainly determined by the possible *coincidence* or *coupling* of the higher-order acoustic modes in

* *Corresponding author: Wolfson School of Mechanical and Manufacturing Engineering, University of Loughborough, Loughborough, Leicestershire LE11 3TU, UK.*

their cavity and the resonant structural modes of the walls [**14**, **25**]. A fundamental study of a two-piece driveline has been reported [**2**, **16**, **17**]. The latter have reported good agreement with the experimental results of reference [**5**] for the case of short-wheel-base rear-wheel-drive trucks, having two-piece driveshafts.

This paper concentrates on the case of long-wheel-base rear-wheel-drive truck drivelines with three-piece driveshaft systems. Additionally, the experimental rig reported in reference [**5**] was a 'static' structure (i.e. non-rotating), subjected to a sudden torsional impulse, and thus devoid of contributions due to inertial dynamics of the drivetrain system. In this paper a new dynamic test rig is reported, which takes into account the inertial dynamics of the drivetrain system, and vehicle inertia under various laden conditions, as well as being subjected to precisely monitored impulsive actions.

2 THE THREE-PIECE VEHICULAR DRIVELINE MODEL

The investigation of clonk is concerned with the determination of conditions that lead to vibro-impact excitation, inducing structural wave propagation and, hence, noise radiation from the lightly damped thin-walled driveshafts of high modal density. The multi-physics problem of this type must be investigated through a combined study of large-displacement inertial dynamics, small-amplitude structural elastodynamics, and acoustic wave propagation.

A multi-body dynamic model, built in ADAMS [**18**] (Fig. 1) is based upon constrained Lagrangian dynamics. This is the mechanical model of the drivetrain system. Component flexibility for the high-modal-density radiated-noise structures has been included through the use of the finite element technique and component mode synthesis method, using NASTRAN [**19**], so that an extension of this study will permit the calculation of radiated noise from the mechanical parts of interest, using either a suitable finite element approach or boundary element method.

The multi-body model consists of all the components of the powertrain system, starting from the transmission input shaft up to and including the rear axle. The inertial properties of all the parts, the constraints introduced by their assembly (modelled with combination of idealized joints), the compliances and restraints of the model and the applied external forces are described in Tables 1 to 4.

The number of degrees of freedom (DOFs) of the multi-body driveline model is obtained, using the Gruebler–kutzbach expression as

$$\begin{aligned}\text{Number of DOFs} &= \text{flexible bodies modes} \\ &\quad + 6(\text{number of rigid parts} - 1) \\ &\quad - \sum(\text{constraints}) \\ &= (91 + 60 + 85) + 6(35 - 1) - 193\end{aligned}$$

Hence, the driveline model has 247 degrees of freedom.

3 METHOD OF FORMULATION AND SOLUTION

The governing equations of motion for an assembly of rigid and elastic constrained bodies are derived

Fig. 1 The multi-body model of the driveline mechanical system

Table 1 Mass and inertia properties of the vehicle driveline model parts

Reference number	Part Name/Description	Mass (kg)	Moments of inertia (kg m^2)		
			I_{xx}	I_{yy}	I_{zz}
1	Transmission input shaft	1.82	9.16×10^{-4}	7.59×10^{-3}	7.59×10^{-3}
2	Transmission main shaft	1.79	4.39×10^{-4}	3.84×10^{-3}	3.84×10^{-3}
3	Transmission countershaft	3.15	8.11×10^{-4}	1.85×10^{-2}	1.85×10^{-2}
4	Transmission output shaft	1.83	4.11×10^{-4}	8.41×10^{-3}	8.41×10^{-3}
5	Transmission output flange	1.02	1.30×10^{-3}	9.80×10^{-4}	9.80×10^{-4}
6	First driveshaft input flange	1.04	1.25×10^{-3}	7.51×10^{-4}	7.51×10^{-4}
7	First driveshaft tube	1.85	2.76×10^{-3}	6.28×10^{-2}	6.25×10^{-2}
8	First driveshaft output flange	0.97	5.27×10^{-4}	9.63×10^{-4}	9.13×10^{-4}
9	Flange yoke	0.85	7.58×10^{-4}	1.00×10^{-3}	5.05×10^{-4}
10	Spider	0.29	1.37×10^{-4}	7.68×10^{-5}	7.68×10^{-5}
11	Second driveshaft yoke	0.95	1.09×10^{-3}	5.51×10^{-4}	1.00×10^{-3}
12	Second driveshaft tube	1.29	1.74×10^{-3}	2.12×10^{-2}	2.12×10^{-2}
13	Second driveshaft output flange	0.97	5.27×10^{-4}	9.13×10^{-4}	9.63×10^{-4}
14	Flange yoke	0.85	7.58×10^{-4}	5.05×10^{-4}	1.00×10^{-3}
15	Spider	0.29	1.37×10^{-4}	7.68×10^{-5}	7.68×10^{-5}
16	Yoke female slip spline	1.16	8.72×10^{-4}	3.37×10^{-3}	3.00×10^{-3}
17	Male spline	1.76	6.79×10^{-4}	6.69×10^{-3}	6.73×10^{-3}
18	Third driveshaft tube	1.72	2.33×10^{-3}	4.99×10^{-2}	4.99×10^{-2}
19	Third driveshaft output flange	0.80	9.42×10^{-4}	8.62×10^{-4}	4.57×10^{-4}
20	Spider	0.35	1.87×10^{-4}	1.04×10^{-4}	1.04×10^{-4}
21	Yoke	0.82	1.32×10^{-3}	1.05×10^{-3}	5.77×10^{-4}
22	Axle flange	1.24	2.34×10^{-3}	1.25×10^{-3}	1.22×10^{-3}
23	Axle drive pinion shaft	2.63	1.11×10^{-3}	9.03×10^{-3}	9.03×10^{-3}
24	Crown wheel-driven gear	4.80	2.00×10^{-2}	3.93×10^{-2}	2.00×10^{-2}
25	Axle differential case	5.62	1.81×10^{-2}	1.90×10^{-2}	2.14×10^{-2}
26	Right-hand side gear (1)	0.57	2.58×10^{-4}	4.33×10^{-4}	2.58×10^{-4}
27	Left-hand side gear (3)	0.57	2.58×10^{-4}	4.33×10^{-4}	2.58×10^{-4}
28	Front side gear (4)	0.25	1.03×10^{-4}	5.89×10^{-5}	1.03×10^{-4}
29	Back side gear (2)	0.25	1.03×10^{-4}	5.89×10^{-5}	1.03×10^{-4}
30	Side gear shaft	0.36	2.25×10^{-5}	4.72×10^{-4}	2.25×10^{-5}
31	left half-shaft	11.44	0.89	1.49×10^{-2}	0.89
32	Right half-shaft	11.44	0.89	1.49×10^{-2}	0.89
33	Left vehicle inertia		Depending on vehicle loading		
34	Right vehicle inertia		Depending on vehicle loading		
35	Ground		–		

from the Lagrange equation for constrained systems in the form

$$\frac{\mathrm{d}}{\mathrm{d}t}\left(\frac{\partial K}{\partial \dot{\xi}_j}\right) - \left(\frac{\partial K}{\partial \xi_j}\right) - F_{\xi_j} + \sum_{k=1}^{n} \lambda_k \frac{\partial C_k}{\partial \xi_j} = 0 \tag{1}$$

where $\{\xi_j\}_{j=1\to 6} = \{x,y,z,\Psi,\theta,\varphi\}^{\mathrm{T}}$ denote the rigid body degrees of freedom, $\{\xi_j\}_{j=1\to 6+m} = \{x,y,z,\Psi,\theta,\varphi,q\}^{\mathrm{T}}$ denote the flexible body degrees of freedom (q are the modal coordinates and m their total number), and λ_k are the Lagrange multipliers for the constraints C_k.

The n constraint functions for the different joints in the driveline model are represented by a combination of holonomic and non-holonomic functions as

$$\begin{bmatrix} C_k \\ \dot{\xi}_j \dfrac{\partial C_k}{\partial \xi_j} \end{bmatrix} = 0 \quad (k = 1 \to n)$$
$$(J = 1 \to 6 \text{ or } 1 \to 6 + m) \tag{2}$$

The multi-body model of the mechanical system is a constrained non-linear dynamics model, incorporating the elastic behaviour of the driveshaft tubes. The dynamic simulation code ADAMS is based on the automatic generation of equations of motion, using constrained Lagrangian dynamics, formulated in the generalized Eulerian 3–1–3 frame of reference. The compliance of the flexible members is given by stiffness and damping matrices obtained during the creation of superelements by modal analysis, as briefly described in the following sections (see also reference [**16**]).

3.1 Component mode synthesis and superelement creation

The introduction of finite element analysis (FEA) techniques (via use of the MSC/NASTRAN code) for the detailed investigation of the behaviour of several parts of the driveline has been considered as necessary, because it achieves two desirable goals.

1. It increases the fidelity of the multi-body model.

Table 2 Constraints between connecting parts in the driveline model

Reference number	Part I	Part J	Constraint type	Number of constraints
1	Transmission input shaft	Transmission main shaft	Fixed	6
2	Transmission main shaft	Ground	Revolute	5
3	Transmission countershaft	Ground	Revolute	5
4	Transmission output shaft	Ground	Revolute	5
5	Transmission output shaft	Transmission output flange	Fixed	6
6	First driveshaft input flange	First driveshaft tube	Fixed	6
7	First driveshaft tube	First driveshaft output flange	Fixed	6
8	First driveshaft output flange	Flange yoke	Fixed	6
9	Flange yoke	Spider	Revolute	5
10	Spider	Second driveshaft yoke	Revolute	5
11	Second driveshaft yoke	Second driveshaft tube	Fixed	6
12	Second driveshaft tube	Second driveshaft output flange	Fixed	6
13	Second driveshaft output flange	Flange yoke	Fixed	6
14	Flange yoke	Spider	Revolute	5
15	Spider	Yoke female slip spline	Revolute	5
16	Yoke female slip spline	Male spline	Translational	5
17	Male spline	Third driveshaft tube	Fixed	6
18	Third driveshaft tube	Third driveshaft output flange	Fixed	6
19	Third driveshaft output flange	Spider	Revolute	5
20	Spider	Yoke	Revolute	5
21	Yoke	Axle flange	Fixed	6
22	Axle flange	Ground	Revolute	5
23	Axle flange	Axle drive pinion shaft	Fixed	6
24	Axle drive pinion shaft	Crown wheel-driven gear	Coupler	1
25	Crown wheel-driven gear	Axle differential case	Fixed	6
26	Crown wheel-driven gear	Ground	Revolute	5
27	Axle differential case	Right-hand side gear (1)	Fixed	6
28	Axle differential case	Left-hand side gear (3)	Fixed	6
29	Axle differential case	Side gear shaft	Fixed	6
30	Side gear shaft	Frond side gear (4)	Fixed	6
31	Side gear shaft	Back side gear (2)	Fixed	6
32	Right-hand side gear (1)	Right-hand half-shaft	Fixed	6
33	Left-hand side gear (3)	Left-hand half-shaft	Fixed	6
34	Right-hand half-shaft	Right vehicle Inertia	Fixed	6
35	Left-hand half-shaft	Left vehicle Inertia	Fixed	6

2. The realistic loads (initial conditions that are required for an external acoustic analysis) may be obtained in a natural way by incorporating an FEA model of a component in the mechanical system, when simulating the in-service events.

The driveshaft pieces (first, second, and third tubes) are major components of the driveline, which have significant flexural behaviour compared with the other parts that have a rather rigid behaviour. By incorporating FEA models instead of rigid bodies for the representation of these components, it is feasible to determine their spectral response during the simulation exercise. Furthermore, the initial conditions (displacements, velocities, loads, etc.) which are required in an acoustic analysis of the driveshaft tubes can be extracted, enabling the determination of the induced sound pressure fields both within and external to each tube.

The most important assumption behind this procedure is the consideration of small, linear elastic deformations relative to a local frame of reference, while this frame of reference undergoes large non-linear global motion. The discretization of a component into finite elements represents the infinite number of DOFs with a finite but very large number of finite element DOFs. The linear deformations of the nodes of this finite element modes, $\boldsymbol{u}$, can be approximated as a linear combination of

Table 3 Restraints and compliances in the driveline model

Reference number	Parts/areas of application	Characteristics
1	First driveshaft tube	Superelement, 91 modes
2	Second driveshaft tube	Superelement, 60 modes
3	Third driveshaft tube	Superelement, 85 modes
4	Total normal backlash, fourth gear set	Experimental data, 63 μm
5	Total normal backlash, second gear set	Experimental data, 75 μm
6	First driveshaft tube angle (around y axis)	Manufacturing data, 4.5°
7	Second driveshaft tube angle (around y axis)	Manufacturing data, 4.9°
8	Third driveshaft tube angle (around y axis)	Manufacturing data 2.8°
9	Third driveshaft tube angle (around z axis)	Manufacturing data, 1.5°

Table 4 Internal and external applied forces

Reference number	Type	Position	Magnitude	Duration
1	Ramp torque	Transmission input shaft	145 N m built up during typical clutch engagement–disengagement (0.1–0.5 s from lowest to highest point of clutch pedal)	
2	Fourth gear impact force	Gear meshing cycle	Hertzian, bending	Impact
3	Second gear impact force	Gear meshing cycle	Hertzian, bending	Impact

a smaller number of shape vectors (or mode shapes), $\boldsymbol{\phi}$, as

$$\boldsymbol{u} = \sum_{i=1}^{m} \boldsymbol{\phi}_i q_i \tag{3}$$

where, m is the number of mode shapes. The scale factors of amplitudes, q, are the modal coordinates.

The main concept of *modal superposition* is that the behaviour of a component with a very large number of nodal DOFs, in a predetermined frequency area, can be captured with a much smaller number of modal DOFs. Thus, the finite element modes can be rewritten in matrix format as

$$\boldsymbol{u} = \boldsymbol{\Phi q} \tag{4}$$

where $\boldsymbol{q}$ is the vector of modal coordinates and the modes ϕ_i are included in the columns of the modal matrix $\boldsymbol{\Phi}$. This matrix is the transformation from the small set of modal coordinates q to the larger set of physical coordinates u.

The determination of the modal matrix $\mathbf{M}$ can be achieved due to the *Craig–Brampton* [**20**] reduction method, which is one of the most general methods of the *component mode synthesis* techniques. The summary of this method is described in the following paragraphs.

1. A set of *boundary* DOFs u_B is defined, which is not to be subject to modal superposition and is preserved exactly in the modal basis.
2. A set of *interior* DOFs u_I is defined.

Additionally, two sets of mode shapes are defined, as follows.

1. The *constraint modes* q_C are static shapes that are obtained by giving each of the boundary DOFs a unit displacement, while holding all other boundary DOFs fixed. There is a one-to-one correspondence between the modal coordinates of the constraint modes and the displacement in the corresponding boundary DOFs: $q_\mathrm{C} = u_\mathrm{B}$.
2. The *Fixed boundary normal modes* q_N, which are obtained by fixing the boundary DOFs and computing a solution of the eigenvalue problem. These modes define the modal expansion of the interior DOFs. The quality of this expansion is proportional to the total number of modes.

According to the above, the relationship between the physical DOFs, the Craig–Brampton modes and their modal coordinates is expressed as

$$\boldsymbol{u} = \begin{pmatrix} u_\mathrm{B} \\ u_\mathrm{I} \end{pmatrix} = \begin{pmatrix} \mathbf{I} & \mathbf{0} \\ \boldsymbol{\Phi}_\mathrm{IC} & \boldsymbol{\Phi}_\mathrm{IN} \end{pmatrix} \begin{pmatrix} q_\mathrm{C} \\ q_\mathrm{N} \end{pmatrix} \tag{5}$$

where $\mathbf{I}$ and $\mathbf{0}$ are unity and zero matrices respectively,

The generalized stiffness and mass matrices are obtained through the transformations

$$\hat{\mathbf{M}} = \boldsymbol{\Phi}^\mathrm{T}\mathbf{M}\boldsymbol{\Phi} = \begin{pmatrix} \hat{\mathbf{M}}_\mathrm{CC} & \mathbf{0} \\ \mathbf{0} & \hat{\mathbf{M}}_\mathrm{NN} \end{pmatrix},$$
$$\hat{\mathbf{K}} = \boldsymbol{\Phi}^\mathrm{T}\mathbf{K}\boldsymbol{\Phi} = \begin{pmatrix} \hat{\mathbf{K}}_\mathrm{CC} & 0 \\ 0 & \hat{\mathbf{K}}_\mathrm{NN} \end{pmatrix} \tag{6}$$

where $\hat{\mathbf{M}}_\mathrm{NN}$ and $\hat{\mathbf{K}}_\mathrm{NN}$ are diagonal matrices and $\hat{\mathbf{K}}$ is a block diagonal matrix.

Since the Craig–Brampton modes are not an orthogonal set of modes, a mode shape orthonormalization procedure is applied. By solving the eigenvalue problem

$$\hat{\mathbf{K}}\boldsymbol{q} = \lambda\hat{\mathbf{M}}\boldsymbol{q} \tag{7}$$

The obtained eigenvectors are arranged in a transformation matrix $\mathbf{N}$ that transforms the Craig–Brampton modal basis to an equivalent orthogonal basis with modal coordinates $\boldsymbol{q}^*$, where

$$\mathbf{N}\boldsymbol{q}^* = \boldsymbol{q} \tag{8}$$

Thus, the effect on the superposition formula is

$$\boldsymbol{u} = \sum_{i=1}^{M} \boldsymbol{\phi}_i q_i = \sum_{i=1}^{M} \boldsymbol{\phi}_i \mathbf{N}\boldsymbol{q}^* = \sum_{i=1}^{M} \boldsymbol{\phi}_i^* \boldsymbol{q}^* \tag{9}$$

where $\boldsymbol{\phi}_i^*$ are the orthogonal Craig–Brampton modes.

Four-noded two-dimensional shell elements with prespecified thickness (1.65 mm) have been used

for the tube walls in the superelement creation. *Clamped–clamped* boundary conditions have been applied to the tube edges to represent the assembly conditions in the vehicular driveshaft system. This has been achieved by using appropriate elements in the tube edges so that a master node (in the edge centre) is rigidly attached to many slave nodes (in the edge circumference) via a type of connection that creates a localised stiffhess in the model (RBE2 elements [**19**]). Since the master node DOFs are independent, this node can be promoted to an *attachment point* and is used to connect the flexible body to the rigid bodies of the multi-body model.

A sufficient number of natural modes have been kept in the superelements creation in order to obtain accurate results in the specified frequency area, where clonk usually occurs (300–5000 Hz). There is no exact rule on how many modes should be kept in the superelement, although a general rule of thumb is that a number of modes that cover at least twice the desired frequency area should be kept. The geometric properties of a tube determine its modal density in this area (its upper limit has been determined as 12 000 Hz in this analysis). Consequently, each tube superelement includes a variety of modes starting from low-frequency bending modes and leading to complicated shapes that are combination of bending–axial and high-frequency torsional modes.

3.2 Meshing cycle gear forces

Calculation of the transmission gear forces between the engaged teeth pair(s) during the meshing cycle is necessary to determine the impact conditions. The geometric characteristics of the *helical* gear teeth affect the dynamics and vibrational behaviour of the mechanical system significantly. Gear *backlash* is either introduced intentionally at the design stages or caused by manufacturing errors and wear. Therefore, the equations of motion of such systems become strongly non-linear. Another complication arises from the variable number of gear teeth pairs, which are in contact simultaneously, causing a variation in the equivalent gear *meshing stiffness*. The dynamics of a gear-pair system, involving backlash and time-dependent mesh stiffness $k(t)$ can be investigated using piece-wise linear equations of motion with time-dependent coefficients. The centres of both gears are constrained against any lateral motion. The meshing stiffness depends on the number and position of the gear teeth pairs, which are in contact (Fig. 2) and is a *periodic* function of the relative angular position of the gears (Fig. 3) [**21–23**]. In this study, a simple and accurate method has been followed, on the basis of ISO 6336

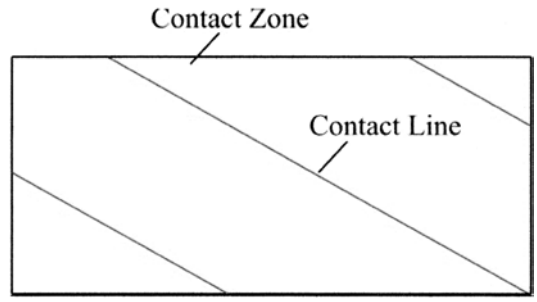

Fig. 2 Zone of contact and contact elements (three teeth pairs in contact)

[**24**]. According to this, the meshing stiffness is calculated, using the value of the *single stiffness k'*, which is the maximum stiffness normal to the helix of a single tooth pair, representing the requisite load over a 1 mm face width directed along the line of action to produce in-line with the load deformation amounting to 1 μm. It is given by the function

$$k' = 0.8\, k'_{\text{th}}\, C_{\text{R}}\, C_{\text{B}}\, \cos\beta \tag{10}$$

For details regarding the calculation of the theoretical single stiffness k'_{th}, gear blank factor C_{R}, and basic rack factor C_{B}, ISO 6336 [**24**] should be consulted. The total meshing stiffness is given by the function

$$k = \text{total length of contact lines} \times k' \tag{11}$$

If the tooth-to-tooth variations (i.e. pitch errors and tooth finishing) are neglected, the fundamental

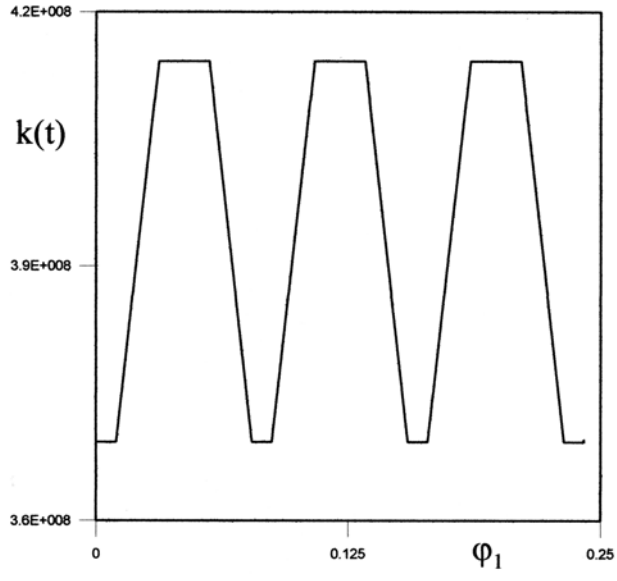

Fig. 3 Stiffness variation with respect to the pinion roll angle

frequency of both of these quantities equals the gear meshing frequency according to

$$\omega_m = n_1\omega_1 = n_2\omega_2 \tag{12}$$

where the integers n_1, and n_2 are the teeth numbers and ω_1 and ω_2 are the angular velocities of the pinion and gear respectively. The force developed between the pair of gears is given by the product $k(t)h(x)$, where $x(t) = R_1\varphi_1(t) - R_2\varphi_2(t)$,$R_1$ and R_2 represent the contact point radii of the gears, $\varphi_1(t)$ and $\varphi_2(t)$ are the two torsional coordinates (rotation angles of the gears) and

$$h(x) = \begin{cases} x-b, & x > b \\ 0, & |x| < b \\ x+b, & x < -b \end{cases}$$

where $2b$ represents the *total normal backlash* between the gear teeth [**25**].

3.3 Introducing vehicular inertia and rolling resistance

Two other important factors must be introduced in the model. Firstly, the rolling resistance as a road input should be included in the model. Secondly, the laden or unladen state of the vehicle as well as its body dynamics play a significant role in dive or squat of the vehicle with tip-in and back-out motions associated with throttle and clutch actions. The various laden conditions of the vehicle significantly influence the driveline behaviour in terms of the torque pulse reflection, which travels through the different components.

The equations of motion for the vehicle body (where $\ddot{x}$ stands for its translational motion) and the rear half-shafts', assembly (where $\ddot{\varphi}$ stands for its rotation) respectively are given as (Fig. 4)

$$\begin{aligned} M\ddot{x} &= F \\ J\ddot{\varphi} &= T - FR \end{aligned} \tag{13}$$

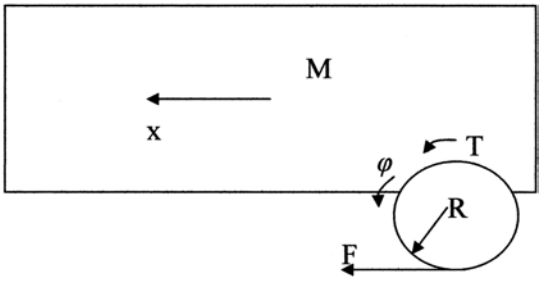

Fig. 4 Free body diagrams of vehicle body and rear half-shafts mechanical system

For pure rolling conditions,

$$\ddot{x} = R\ddot{\varphi} \tag{14}$$

and, by substituting it in the previous set of equations, this yields

$$(J + MR^2)\ddot{\varphi} = T \tag{15}$$

This means that the body of the vehicle could be 'transferred' as an *equivalent amount of inertia* to the rear wheel assembly by adding in the assembly inertia the quantity MR^2, which obviously varies with respect to the different vehicular loading conditions.

4 EXPERIMENTAL RIG

To capture the transient behaviour of the clonk phenomenon, it is essential to introduce inertial dynamics of the drivetrain system under conditions that promote impact loading in the various lash zones. The previously so-called 'static experimental rig' [**5**] is inadequate in the sense that the transient nature of the phenomenon is introduced without regard to the actual inertial dynamics of the drivetrain system, although very good agreement in qualitative terms was obtained between rig-based experiments and *in-situ* vehicle tests carried out at the Ford Research Centre in Dunton. Many issues were encountered during the rig design. They included provisions for alignment of the drivetrain system to replicate vehicle conditions closely, as well as vibration isolation from environmental effects, and from those that are introduced by the actuation mechanisms, other than those that are encountered under similar vehicle-testing conditions. Method of actuation of the rig and imposition of impulse, such as throttle action or clutch activation, is of paramount importance. Finally, proper provisions had to be made with regard to the repeatability of the actuating signals, their conformance to driver or vehicle behaviour, and the reproducibility of the actual variations.

It was decided to use an electric motor for the drivetrain actuation, as this provides the opportunity to apply fully controllable torque conditions compared with those of an internal combustion engine. The motor has the appropriate specifications in order to accelerate the drivetrain up to the testing speed of 1500 r/min with a maximum torque of 145 N m, which correspond to the observed and recorded clonk conditions on the real vehicle, when engaged in the second gear. The smoothness in the motor's performance is achieved by using an inverter, which produces controllable torque rise and fall

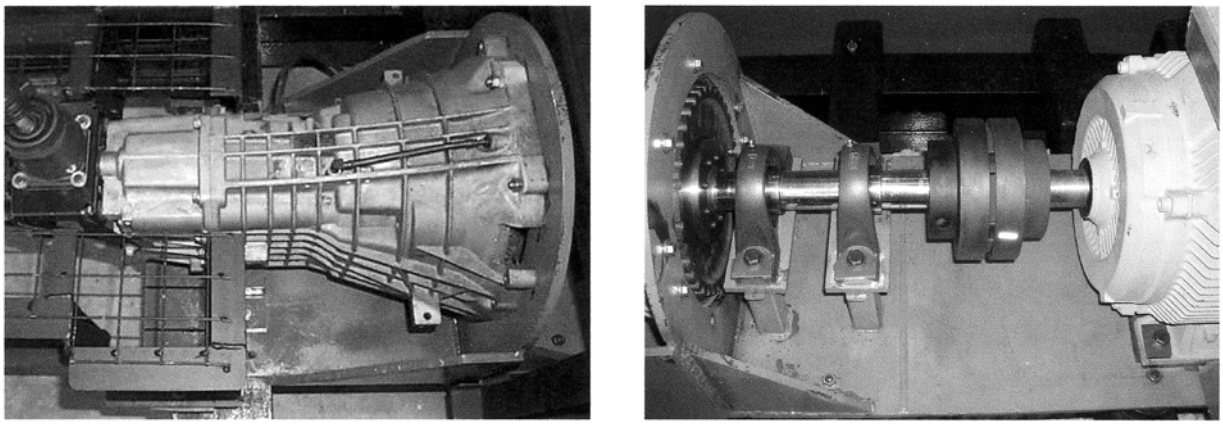

Fig. 5 The complete gearbox unit and motor–gearbox coupling

rates. Since the motor is directly coupled to the gearbox and through this connection transmits the required torque to the drivetrain, a suitable coupling unit was chosen to ensure the smooth torque transmissibility and to limit the transmission of the torsional vibrations of the motor itself. The alignment in the connection of the gearbox and the motor was achieved by building the gearbox and the block units together on a solid plate. The complete unit is shown in Fig. 5.

An existing hand-brake system used on the actual vehicle was modified, using an electronic control unit, and calibrated in order to operate in a repeatable manner and to introduce various laden states of the vehicle by applying resistance via the rear axle.

The main supports of the rig are two 3.5 m and two 1.5 m I-section beams of 210 mm height, connected together (each 3.5 m beam to a 1.5 m beam) and bolted to the laboratory floor by raw bolts and elastomeric pads interfering between the beams and the floor in order to isolate the rig and to minimize vibration transmissibility. The electric motor is mounted on cross-beams through pads for vibration isolation. The cross-beams are mounted on to the I-section beams. For better alignment of the coupling–flywheel–gearbox assembly, the transmission bell housing and the coupling system have been fixed to a bed-plate, which in turn has been mounted on to cross-beams through pads. Consideration has been given to the angles that the driveshafts assemble together and on to the rear axle. The rear axle is hung from the mounting brackets that are also mounted on the I-section beams through pads. A top view of the drivetrain rig is shown in Fig. 6. To capture driveline vibration and noise, a variety of instruments are used, including laser vibrometers, microphones, and accelerometers. The positions of all monitoring equipment are schematically shown in Fig. 7.

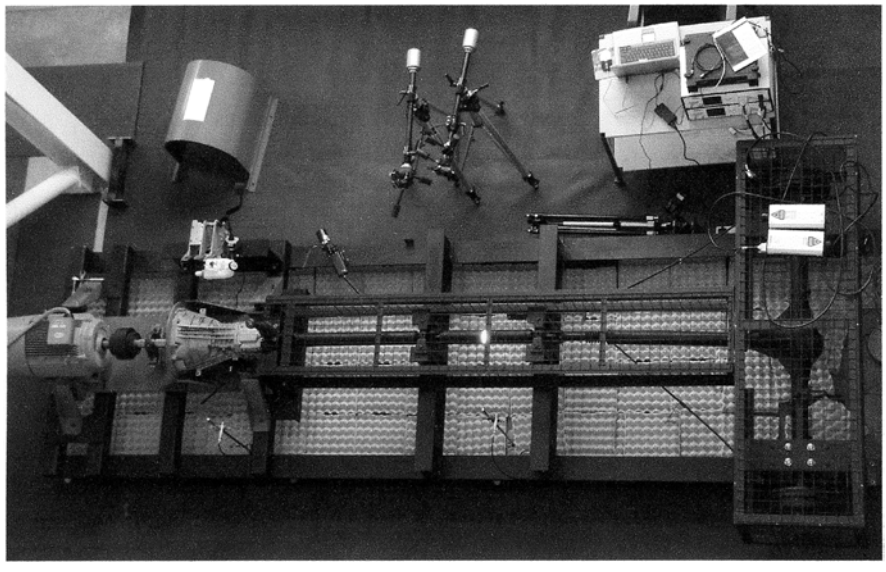

Fig. 6 Top view of the drivetrain experimental rig

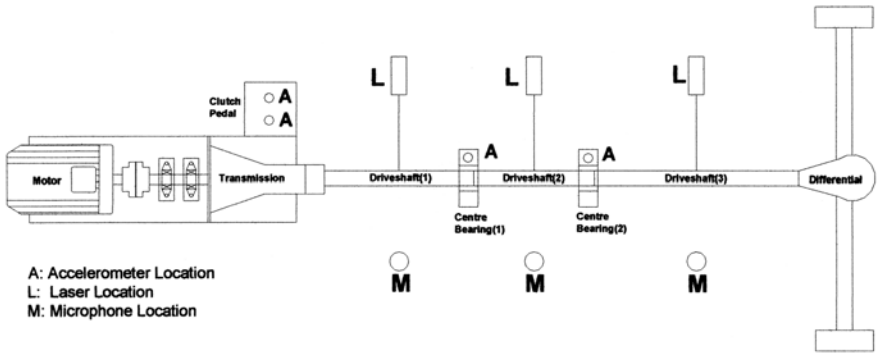

Fig. 7 Schematic layout of the rig, showing the positions of various pick-ups

5 SIMULATION STUDIES, EXPERIMENTAL RESULTS, AND DISCUSSION

A simulation study of sudden torque application is carried out with the flexible multi-body dynamic model of the drivetrain system. The central processing unit time was approximately 4.5 h on a 1.8 GHz Pentium IV desktop computer for 140 ms of system simulation, in 140 000 computation time intervals.

Figure 8 reveals the dominant lateral modes of the driveshaft pieces, when the drivetrain system is

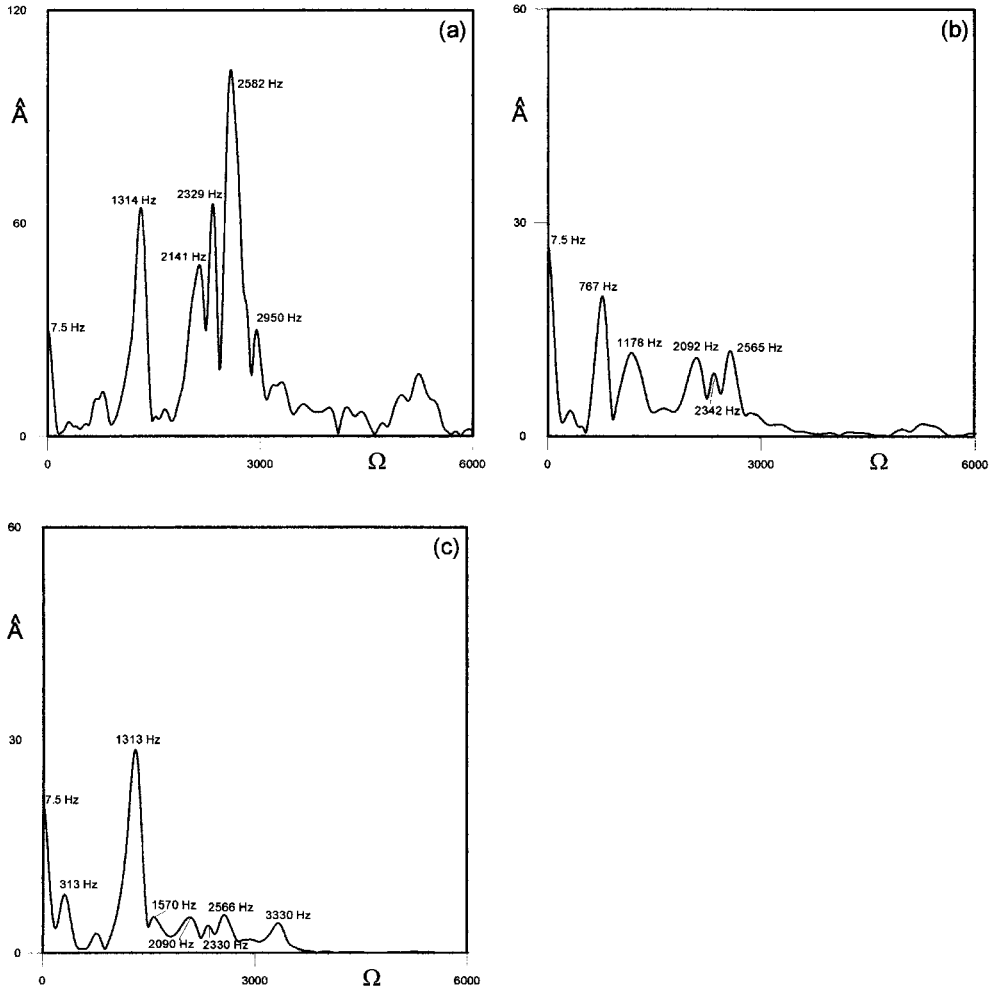

Fig. 8 Fast fourier transform spectra of the lateral time history responses corresponding to the (a) front, (b) middle and (c) rear shafts

subjected to a sudden torque demand as in throttle tip-in from coast to drive condition. These graphs are the amplitudes of the fast Fourier transform spectra of the time history responses obtained on the surface of the numerical drivetrain model. The applied torque has a magnitude of 145 N m over 200 ms. Impact time under this condition is in the region 1–5 ms.

The second driveshaft tube is splined to the rear tube and has freedom to float (i.e. is not axially

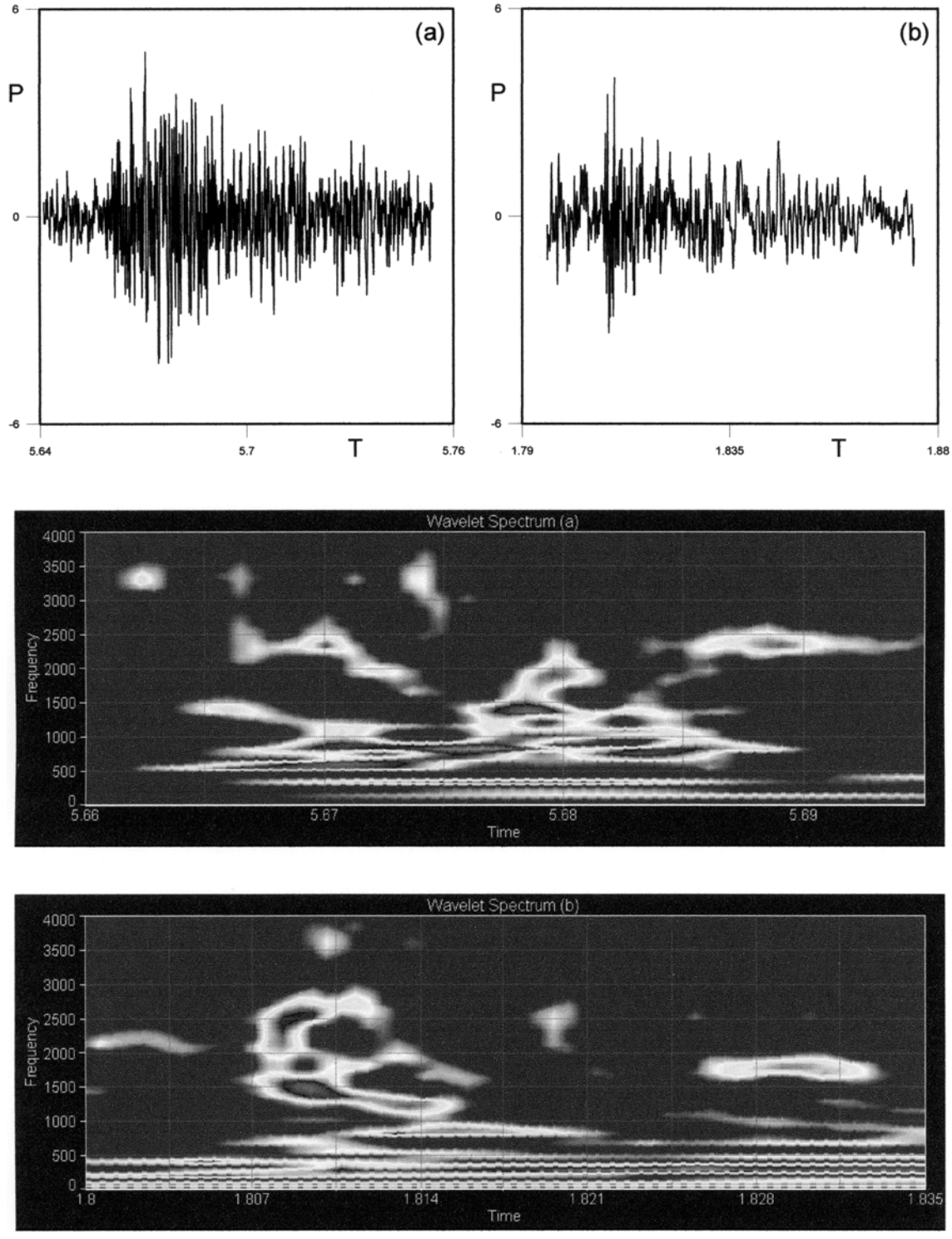

Fig. 9 Typical raw clonk noise signals (pressure levels) and wavelet maps, corresponding to the (a) front and (b) rear driveshaft tubes

constrained). This means that, at the natural frequencies of the first and third tube, the middle tube acts like a mass similar to a spring–mass system with impact transferred to this 'mass' as a forcing frequency other than its own natural modal response (this appears as 2082 and 2294 Hz). Since the middle tube is not constrained (which is physically impossible, because of the angle between the front and rear driveshafts), its torsional mode is not expected to be observed. This, in fact, is the case (its torsional mode is at 3644 Hz). It, therefore, follows the torsional oscillations of the first tube (i.e. at 2671 Hz). The third tube has very close torsional mode to the first (for both around 2770 Hz for the first tube and 2724 Hz for the third). It is noticeable that only a few of the modes present in the spectra are the *breathing modes*, namely 2304 Hz, 2354 Hz, and 2667 Hz for the front shaft, 2082 Hz and 2994 Hz for the middle shaft, and 2347 Hz and 3311 Hz for the rear shaft [**16**]. This means that these are the only modes of the driveshaft pieces that contribute to the clonk noise (i.e., at these modes, the tubes act as loudspeakers).

The above numerical results agree well with the experimental measurements shown in Fig. 9, obtained by monitoring the dynamic experimental rig under identically imposed conditions. The first two graphs in Figs 9(a) and (b) show the sound pressure levels, corresponding to the front and rear tubes respectively. There is, clearly, a reduction in the noise level as the impact wave propagates towards the differential. This is also in agreement with the energy power distribution between the spectra in Figs 8(a) and (c). Furthermore, in Fig. 9, the wavelet maps of the noise levels reveal a rich spectrum that includes a variety of frequencies. Some of these come from the transmission and the differential, because of the impacting gear teeth pairs during the generation of the clonk noise, and the reason for their absence in the numerical predictions, which mainly examines the contributions due to the driveshaft pieces. However, the main breathing modes of the tubes (observed in the numerical analysis) are present, revealing a clear contribution from the driveshaft tubes in the clonk noise signal. Finally, it is worth mentioning that the lowest torsional rigid body mode of the driveline (commonly known as shuffle) is present in the analysis spectra, confirming the clear relation between the two NVH phenomena at the extremes of the drivetrain spectra of vibration: shuffle and clonk.

ACKNOWLEDGEMENTS

The authors wish to express their gratitude to Ford Motor Company, MSC Software, and the Vehicle Foresight Directorate (the Engineering and Physical Sciences Research Council and the Department of Trade and Industry) for the sponsorship and financial support extended to this research project.

REFERENCES

1 **Rahnejat, H.** *Multi-body Dynamics: Vehicles, Machines and Mechanisms*, 1998 (Professional Engineering Publishing Limited, Bury St Edmonds and London) (Society of Automotive Engineers, Warrendale, Pennsylvania).

2 **Arrundale, D., Hussain, K., Rahnejat, H.,** and **Menday, M. T.** Acoustic response of driveline pieces under impacting loads (clonk). In Proceedings of the 31st International Symposion on *ATA (ISATA)*, Dusseldorf, Germany, 1998, pp. 319–331.

3 **Biermann, J. W.** and **Hagerodt, B.** Investigation into the clonk phenomenon in vehicle transmission – measurement, modelling and simulation. *Proc. Instn Mech. Engrs, Part K: J. Multi-body Dynamics*, 1999, **213**(K1), 53–60.

4 **Menday, M., Rahnejat, H.,** and **Ebrahimi, M.** Clonk: an onomatopoeic response in torsional impact of automotive dirvelines. *Proc. Instn Mech. Engrs, Part D: J. Automobile Engng*, 1999, **213**, 349–357.

5 **Vafaei, S., Menday, M. T.,** and **Rahnejat, H.** Transient high-frequency elasto-acoustic response of a vehicular drivetrain to sudden throttle demand. *Proc. Instn Mech. Engrs, Part K: J. Multi-body Dynamics*, 2001, **215**, 35–52.

6 **Fothergil, D. J.** and **Swierstra, N.** The application of non-linear displacements modeling techniques to an automotive driveline for the investigation of shunt. Berichte 1007, Verein Dentscher Ingeniewe, 1992, pp. 163–179.

7 **Hawthorn, J.** A mathematical investigation of driveability. Report C420/003, Institution of Mechanical Engineers, 1995.

8 **Rooke, G., Chan, E. A.,** and **Crossley, P. R.** Computer modeling of a vehicle powertrain for driveability development. Report C462/31/035, Institution of Mechanical Engineers, 1995, pp. 1–9.

9 **Farshindiafar, A., Ebrahimi, M., Rahnejat, H.,** and **Menday, M. T.** High frequency torsional vibration of vehicular driveline systems in clonk. *Int. J. Veh. Des.*, 2002, **9**, 127–149.

10 **Krenz, R.** Vehicle response to throttle tip in/tip out. SAE paper 850967, 1985.

11 **Tobler, W.** and **Tsangerides, M.** Dynamic behaviour of a torque converter with centrifugal bypass clutch. SAE paper 850461, 1985.

12 **Petri, H.** and **Heldingfeld, D.,** The hydraulic torsion damper – a new concept for vibration damping in powertrains. SAE paper 892447, 1989.

13 **Kelly, P., Menday, M., Rahnejat, M.,** and **Ebrahimi, M.** Powertrain refinement: A combined experimental and multi-body dynamics analysis approach. In Proceedings

of the 8th Aachener Kolloquium, Aachen, Germany, 1999, pp. 1079–1094.
14 **Fahy, F. J.** *Sound and Structural Vibration: Radiation, Transmission and Response*, 1985 (Academic Press, New York).
15 **Norton, M. P.** *Fundamentals of Noise and Vibration Analysis for Engineers*, 1989 (Cambridge University Press, Cambridge).
16 **Theodossiades, S., Gnanakumarr, M., Rahnejat, H.,** and **Menday, M.** Mode identification in impact-induced high-frequency vehicular driveline vibrations using an elasto-multi-body approach. *Proc. Instn Mech. Engrs, Part K: J. Multi-body Dynamics*, 2004, **218**, 81–94.
17 **Theodossiades, S., Gnanakumarr, M., Rahnejat, H.,** and **Menday, M.** Combined multi-body dynamics, structural modal analysis and boundary element method to predict multi-physics interactions of driveline clonk. In Proceedings of the 3rd International Multi-body Dynamics Symposium on *Monitoring and Simulation Techniques*, Loughborough, UK, 2004, pp. 373–387.
18 *Adams/View, Solver Reference Manual, Version 12.0*, 2002 (Mechanical Dynamics Inc., Ann Arbor, Michigan).
19 *Patran/Nastran Reference Manual, Version 2001* (MSC Software, Santa Ana, California).
20 **Craig, R. R.** and **Brampton, M. C. C.** Coupling of sub-structures for dynamics analysis. *Am. Inst. Aeronaut. Astronaut.*, 1968, **6**(7), 1313–1319.
21 **Chen, Y. C.** and **Tsay, C. B.** Stress analysis of helical gear set with localized bearing contact. *Finite Elements Analysis des.*, 2002, **38**, 707–723.
22 **Choi, M.** and **David, J. W.** Mesh stiffness and transmission error of spur and helical gears. SAE paper 901764, 1990.
23 **Zhang, J. J., Esat, I. I.,** and **Shi, Y. H.** Load analysis with varying mesh stiffness. *Computers Structs*, 1999, **70**, 273–280.
24 ISO 6336. Calculation of load capacity of spur and helical gears, 1996 (International Standardization Organization, Geneva).
25 **Theodossiades, S.** and **Natsiavas, S.** Non-linear dynamics of gear-pair systems with periodic stiffness and backlash. *J. Sound Vibr.*, 2000, **229**(2), 287–310.

APPENDIX

Notation

C_B	basic rack factor
C_k	constraint functions
C_R	gear blank factor
F	resistive force in the wheels of the rear axle
F_{ξ_i}	generalized applied forces projected on ξ
J	inertia of the rear axle assembly
k'	single gear stiffness
k'_{th}	theoretical single gear stiffness
$k(t)$	Gear teeth pair contact stiffness
K	kinetic energy
m	number of independent coordinates
M	vehicle body mass
n	number of constraints
n_1, n_2	numbers of teeth on the pinion and driven gear respectively
q	modal coordinates
R	wheel radius
R_1, R_2	pitch radii of the pinion and driven gear respectively
T	transmitted torque in the rear axle
$\boldsymbol{u}$	linear nodal deformation vector
X,Y,Z	translational degrees of freedom
β	helix angle at the reference cylinder
λ_k	Lagrange multipliers
ξ_j	generalized coordinates
$\boldsymbol{\phi}$	deformation shape vector
$\varphi_{1,2}$	rotation angles of the pinion and driven gear respectively
$\boldsymbol{\Phi}_{IC}$	physical displacements of the interior degrees of freedom in the constraint modes
$\boldsymbol{\Phi}_{IN}$	physical displacements of the interior degrees of freedom in the normal modes
Ψ, θ, φ	Euler angles
ω_m	gear meshing frequency
ω_1, ω_2	angular velocities of the pinion and driven gear respectively